International Symposium
On Turbulence and Shear Flow
Phenomena (TSFP-9)
June 30 - July 3, 2015 *Melbourne, Australia*

Studies of the large-scale structure in adiabatic and moderately-wall-heated subsonic boundary layers

Stanislav Gordeyev
Department of Aerospace and Mechanical Engineering
University of Notre Dame
Notre Dame, Indiana, 46556, USA
sgordeye@nd.edu

Adam E. Smith
Department of Aerospace and Mechanical Engineering
University of Notre Dame
Notre Dame, Indiana, 46556, USA
asmith31@nd.edu

Theresa Saxton-Fox
Department of Mechanical and Civil Engineering
California Institute of Technology,
Pasadena, California, 91125, USA
tsaxtonf@caltech.edu

Beverley McKeon
Graduate Aerospace Laboratories
California Institute of Technology,
Pasadena, California, 91125, USA
mckeon@caltech.edu

ABSTRACT

Simultaneous velocity-optical measurements in subsonic boundary layers were conducted in order to investigate the relationship between the instantaneous 2-D wavefronts, measured by different optical sensors, the Malley probe and 2-D Shack-Hartmann sensors, and the instantaneous large-scale structure along a wall-normal plane, using PIV in both incompressible and compressible subsonic boundary layers. These systematic studies of the instantaneous relation between the large-scale boundary layer structure and its aero-optical signature provide additional understanding of the instantaneous dynamics of the large-scale structure at subsonic and transonic speeds.

INTRODUCTION

Large-scale structures, located in the outer part of the subsonic boundary layer (BL) carry an important role in boundary layer dynamics, responsible for entrainment process and, via a link with small-scale structures near the wall, for instantaneous drag near the wall, to mention a few (Marusic et al., 2010). While there exists a large body of experimental research about the large-scale structures (Smits et al., 2011), there are open questions about their topology, dynamics and the interaction with the near-wall structures.

Traditionally, large-scale structures are characterized by the velocity field, which is measured using hot-wires or a PIV technique. These techniques give either detailed temporal information in a few spatial points (hot-wires) or potentially time-resolved spatial velocity field information in a plane (particle image velocimetry, PIV). In order to get instantaneous three-dimensional information about the structure, one has to resort to rather complex techniques, like tomographic-PIV (Elsinga et al., 2006) or plenoptic (Farbinger and Thurow, 2012) techniques, for example.

An alternative way to non-intrusively study the characteristics of large-scale structures in boundary layers is to measure related density distortions. Turbulent density fluctuations that are present in the region immediately around an aerodynamic vehicle alter the local speed of light passing into and/or out of the aircraft through the turbulent region. This phenomenon is known as the aero-optic problem (Wang et al., 2012). As planar wavefronts propagate through these unsteady density distributions, they get distorted and these distortions can be accurately measured by various wavefront sensors.

APPROACH

In this work, we leverage both velocimetry and optical techniques to characterize large scale structure in incompressible and compressible turbulent boundary

layers. A brief introduction to the optical techniques is given below.

The levels of optical wavefront distortions can be quantified by the Optical-Path-Difference, *OPD*(*x,z,t*), (Wang at el, 2012)

$$OPL(x,y,t) = K_{GD}\int_a^b \rho'(x,y,z,t)dy \qquad (1)$$

where K_{GD} is the Gladstone-Dale constant and the integration is performed along the beam propagation axis, *y*.

Sutton (1969) introduced the so-called 'linking equation' relating turbulence quantities and levels of optical distortions, given as,

$$OPD_{rms}^2 = 2K_{GD}^2 \int \rho_{rms}^2 \Lambda_\rho(y)dy \qquad (2)$$

where OPD_{rms} is the spatial root-mean-square of the *OPD*, $\rho_{rms}(y)$ is the root-mean-square density fluctuation profile along the beam direction, and $\Lambda_\rho(y)$ is the density correlation length in the wall-normal direction. Using the linking equation (2), a model for time-averaged levels of aero-optical distortions was developed and it was shown to correctly predict OPD_{rms} over a wide range of Mach numbers (Gordeyev et al., 2014), as well as identifying the large-scale structures as main source of aero-optical distortions.

As stated before, in incompressible, wall-heated boundary layers density fluctuations occur due to total temperature variations. Above M = 0.3, compressibility effects can also change the density. If the total temperature is assumed to be a constant, which is equivalent to zero pressure fluctuations, the density fluctuations, ρ', in boundary layers are due to the static temperature fluctuations, *T*', (adiabatic cooling/heating). Using this assumption, the instantaneous version of the Strong Reynolds Analogy (SRA) (Morkovin, 1962) leads to a relationship with the velocity field,

$$CpT'(\vec{x},t) = -\overline{U}u'(\vec{x},t) \qquad (3)$$

Here the velocity fluctuations, *u*', inside the boundary layer are assumed to be much smaller than the local mean flow, $\overline{U}$.

The time-averaged version of SRA was shown to correctly estimate the time-averaged levels of BL aero-optical distortions (Gordeyev et al., 2014). If instantaneous wavefronts and velocity fields are known, it is possible to estimate the validity of the instantaneous version of SRA by comparing measured wavefronts and estimated wavefronts from instantaneous velocity field via equations (1) and (3). Cress et al (2010) showed that if the boundary layer wall is moderately-heated relative to the freestream density, it will not modify the underlying velocity structure. Instead, moderate heating will simply introduce passive temperature markers in the boundary layer and effectively amplify aero-optical levels, such that the OPD can be described by (Cress, 2010; Gordeyev et al., 2015)

$$OPD \sim M^2 + \Delta T/T_\infty \qquad (4)$$

Comparison of properly normalized optical spectra of an incompressible, M ~ 0.05, slightly heated boundary layer taken in the Caltech tunnel and a compressible, M = 0.6, adiabatic-wall boundary layer taken in the Notre Dame tunnel are presented in Figure 1. The optical spectra are nearly identical, except for the high-frequency, small-scale range due to the Reynolds number mismatch in experiments. As these slightly-heated regions will have lower density, it is possible to measure resulted density fluctuations by measuring *OPD* with good spatial and temporal resolution using very sensitive wavefront sensors. In other words, by introducing moderate-temperature mismatch between the wall and the boundary layer, it is possible to *thermally tag* and measure three-dimensional large-scale structures in *incompressible* boundary layers. By heating up or cooling off only parts of the upstream wall, it is possible to introduce thermal internal layers (Smith, 2015), allowing study of only a part of the structure inside the sub-layer.

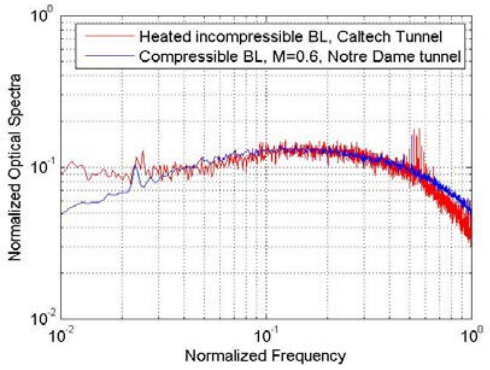

Figure 1. Comparison between optical spectra for the moderately-heated incompressible boundary layer and the compressible, M=0.6, boundary layer.

Two simultaneous wavefront-velocity experiments were conducted at a low subsonic speed at California Institute of Technology (Caltech), using the moderately-heated approach and at a compressible subsonic speed at University of Notre Dame. A Malley probe, consisting of two laser beams passing through the boundary layer and separated by a small streamwise distance (Gordeyev et al., 2014), was used in the Caltech experiments to characterize optical distortions and obtain an appropriate mean convection velocity. From the time series of the deflection angles, 1-D wavefront information in the streamwise direction can be reconstructed (Gordeyev et al., 2014), representing the aero-optical distortion integrated through the boundary layer. A Shack-Hartmann sensor, consisting of a high-speed camera with a lenslet array (Platt and Shack, 2001) was used to obtain more detailed, two-dimensional aero-optical information in the Notre Dame experiments, specifically, the two-dimensional, time-resolved *OPD*.

A simplified inverse problem to describe the deflection of the Malley probe beams was formulated and investigated by using the instantaneous deflection to infer the (integrated) density variations across the boundary layer profile and comparing that profile to the observed velocity field. Solving the full inverse problem is difficult, as the Malley probe gives an integral measure of density fluctuations and the instantaneous density profile is complex. By making a simplifying assumption, progress

can be made on this inverse problem. If it is assumed that there is only one sharp gradient in density along the optical path (i.e. there is some interface between `mixed' and `unmixed' in the wall-normal direction), the inverse problem can be solved and the structure responsible for the optical distortion identified.

The SRA was used to investigate the relationship between optical distortion and the velocity field, comparing the *OPD* implied by the velocity field and equation (3) with the one-dimensional *OPD* from the Shack-Hartmann sensor at the location of the PIV plane.

Both approaches yield local, temporal information about the characteristics of the large-scale structures causing optical distortion.

EXPERIMENTAL SET-UP

Simultaneous WF-PIV set-up: Caltech

Experiments were conducted in the Merrill Wind Tunnel facility at Caltech under the following flow conditions: Re_θ = 2100, M_∞ = 0.03, θ = 2.3 cm, with the wall heated to 20 °C above the free stream temperature. Wavefront measurements were conducted using a Malley probe, which measures deflection angles of two small-aperture beams, aligned in the streamwise direction, shown in Figure 2. Specifically, the Malley probe measurements were obtained 1.04 m (40δ) downstream of the boundary layer trip, with the two beams separated by 5.6 mm and sampled synchronously at 30 kHz. PIV measurements were obtained in the streamwise/wall-normal plane at the same spanwise location and centered on the spanwise location of the Malley probe measurements. A commercial LaVision PIV system consisting of a double-pulsed Yag laser firing at 1 kHz with a 15 ms delay between pulses, and a CCD camera with resolution 1024×1024 pixels and field of view 32×32 mm^2 was used to obtain with velocity fields simultaneously with the Malley probe OPD data. Figure 4(a) shows the location of the Malley probe beams within the PIV field of view.

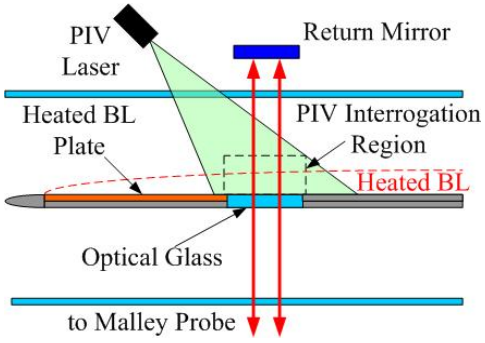

Figure 2. Schematic of the simultaneous Velocity-Wavefront measurements using Malley probe and a heated BL plate at Caltech.

Simultaneous WF-PIV set-up: Notre Dame

Measurements were obtained in the Hessert Transonic Wind Tunnel (TWT) at the University of Notre Dame. The TWT is a continuous flow indraft wind tunnel with an inlet contraction ratio of 150:1, and a cross-section of 10 cm × 9.9 cm in the tunnel test section, which is constructed of Plexiglas. The test section was 160 cm in length from the end of the inlet to the diffuser, with optical windows installed on the upper and lower walls from 130 cm to 150 cm. Freestream velocity was measured using a static pressure port just upstream of the optical window, and was held constant at M = 0.4 for the duration of the measurements.

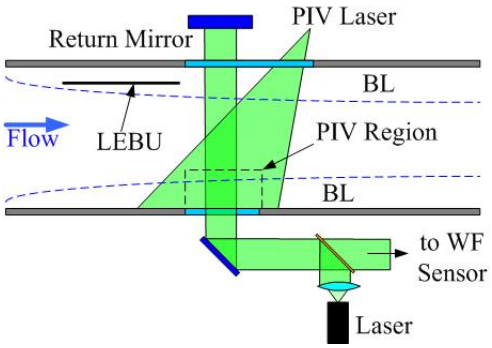

Figure 3. Schematic of of the simultaneous Velocity-Wavefront measurements using Shack-Hartmann 2-D wavefront sensor at Notre Dame.

The experimental set-up at Notre Dame, shown in Figure 3, was similar to the one at Caltech with two major differences. Unlike the 1-D wavefronts, measured with the Malley probe at Caltech, full circular 2-D wavefronts, resolved in both the streamwise (x) and the spanwise (z) directions, were collected using a high-speed Shack-Hartmann wavefront sensor. The wavefront aperture was 50 mm. The second difference was that both boundary layers on the opposite tunnel walls were optically-aberrating. In order to minimize the optical effect of the upper boundary layer, a Large Eddy Break Up (LEBU) device l = 72 mm, h = 11 mm device was mounted on the upper wall of the BL development section to reduce the level of optical aberrations caused by the upper BL. Its trailing edge was located 2.6 cm upstream of the start of the optical window. Previous measurements (Smith, 2015) showed that the LEBU device reduced the aero-optical distortions of the upper boundary layer by a factor of 1.7.

Velocity data were acquired at a rate of 2 kHz using a commercially available 2-D PIV LaVision system in double-pulse, double-frame mode. The laser sheet was aligned along the tunnel centerline, and the frame resolution of the camera was 768×768, with a field of view of approximately 100 mm. The time interval between laser pulses for each measurement was 10 μs. The PIV image pairs were cropped and processed in DaVis 8.2 in order to calculate the velocity vector field at intervals of 0.53 mm in the streamwise and wall-normal directions.

Wavefront measurements with the spatial resolution of 40×40 subapertures were simultaneously acquired using a Shack-Hartmann sensor, which consisted of a high-speed camera (Phantom v1611) with a mounted lenslet array, 3 μs after the first laser pulse, so as to have wavefront data that closely corresponded to each image pair used to calculate the velocity field. The shutter duration for the Shack-Hartmann sensor was only 0.452 μs , and the points at which wavefront measurements were obtained were

distributed at 1.2 mm intervals in the streamwise and spanwise directions. The aperture diameter of the wavefront beam was approximately 5 cm, with its upstream edge passing through the optical window at x = 133 cm. (This gives a distance of approximately 5.6 cm between the LEBU trailing edge and the upstream edge of the Shack-Hartmann beam).

The boundary layer thickness, δ_{99}, at the measurements location was found to be approximately 15.6 mm. Integration of the velocity profiles, collected with PIV system gave δ^* to be 2.4 mm and θ = 1.74 mm. Based on these values, Re_τ = 4,780 and Re_θ = 15,500

Time-averaged levels of *OPD* from the velocity data were found approximately 25% less than the OPDrms, calculated from wavefronts. The difference was attributed to the presence of the optically-weakened upper boundary layer.

RESULTS

Incompressible BL

Correlation of the instantaneous deflection of the two Malley probe beams identifies flow velocities corresponding to the outer part of the boundary layer, with an average convection velocity of 0.8 U_∞. This result is in good agreement with previous studies (Gordeyev et al., 2014) and results from the incompressible boundary layer experiments reported here.

A representative theoretical density interface resulting from the simplified inverse problem described above, together with projection of the temporal signal to the spatial domain using the local convection velocity from the Malley probe signal is superimposed on the corresponding PIV image in Figure 4(b), and can be seen to exhibit reasonable correlation with the location of vortical activity.

Compressible BL

For each velocity field, the estimated 1-D slice of the wavefront was calculated using equations (1) and (3). The resulted wavefronts (not shown) were compared to the 1-D slices of the measured wavefronts along the centerline (Figures 5 and 6). Instances with significant local differences between the estimated and actual wavefronts were investigated. As the estimated wavefronts rely on SRA, these instances should correspond to the cases where the pressure/total temperature fluctuations are not negligible. Two events in the measured wavefront slices were considered, local *OPD* minima and maxima, and the velocity fields were inspected in attempt to identify the probable relation between the wavefront minima/maxima and a corresponding velocity features.

Local *OPD*-minima. Several representative flow fields, when the local wavefront minimum was observed, are shown in Figure 5. The upper plot shows the actual 2-D *OPD* (in false color) and the 1-D *OPD* slice (black line). The bottom plot shows the instantaneous U-velocity with the mean convection velocity of optical disturbance, $0.82U_\infty$, subtracted (velocity vectors), superimposed with the instantaneous fluctuating u-field (false color). It was observed that in most cases the local *OPD* minimum corresponds to the presence of the large-scale, order of δ, structure, which is characterized by negative u-fluctuations near the wall and positive u-fluctuations away from the wall. Such large-scale structure has been observed to correspond to the signature of a packet of hairpin vortical structures by many other researchers (Adrian, 2007, Hutchins et al., 2005, for instance). There is some evidence of vortical motion reminiscent of hairpin heads in the PIV images.

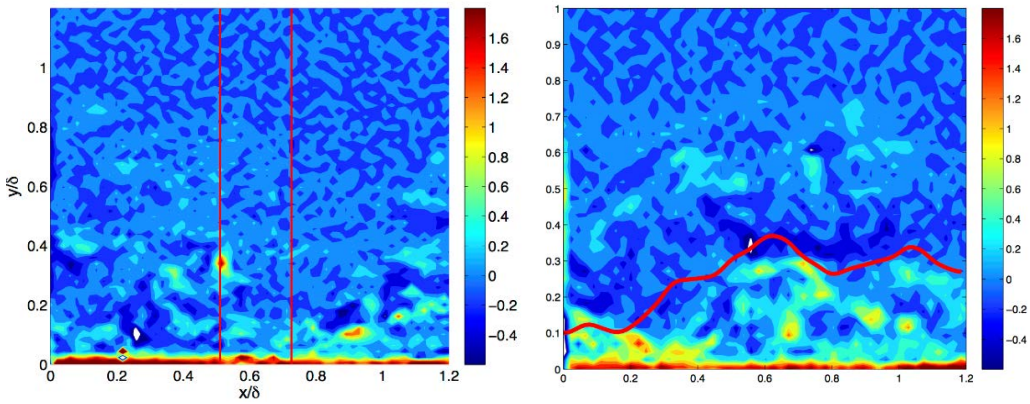

Figure 4. Malley probe/PIV experiments. (a) Example PIV image showing the field of view centered on the Malley probe beam locations (identified with red vertical lines). Color isocontours show instantaneous regions of concentrated spanwise vorticity. (b) The interface reconstructed from simplified inverse problem for the Malley probe data (red line) shows correlation with instantaneous vortical activity.

The discrepancy between the measured and actual wavefronts inside these large-scale structures suggests that the pressure variations are not small inside these structures. It has been shown that the pressure fluctuations in shear layers with well-defined vortical structures significantly contribute to the overall aero-optical distortions (Fitzgerald and Jumper, 2004). So it is plausible to assume that a packet of vortical structures in the boundary layer might have an associated lower pressure region inside, leading to the observed discrepancy between the SRA and measured *OPD*.

As wavefronts are integrals of the density field, analysis of the spanwise extent of the local minima provides non-intrusive optical measurements of the instantaneous spanwise size of the large-scale structures.

For instance, from Figure 5, a typical spanwise extent is found to be approximately 0.5δ with a typical streamwise extend of ~1δ. Again, these observations of predominantly streamwise-elongated large-scale structures are consistent with findings in the literature (e.g. Hutchins et al, 2005).

Local *OPD*-Maxima. A similar analysis was performed to find a flow structure that corresponds to the local *OPD*-maximum. Several examples of velocity fields with related *OPD*s are shown in Figure 6. The velocity field vectors are plotted the same way, as in Figure 5, but this time a false-color map shows the v-fluctuations. It was observed that the most local *OPD* maxima are related to compact regions of large positive v-fluctuations, residing mostly in the outer portion of the boundary layer. One plausible explanation of why these ejection-like, positive vertical-velocity regions corresponds to the local *OPD* maximum is that these vertical velocities will increase the local turbulent thickness of the boundary layer and form a "bulge" in the boundary layer interface; consequently, the upper limit of integration in equation (1) and therefore the *OPD*-value would increase. As no obvious large-scale vortical structure was observed in these representative velocity fields, local *OPD*-maxima are most probably related to the local increase of the boundary layer thickness.

Again, assuming that the streamwise and the spanwise size of the wavefronts at the local maxima are related to the size of these vertical-velocity regions, wavefronts in Figure 6 suggest that these interface "bulges" are approximately 0.7δ in both streamwise and spanwise directions.

Finally, instances where the measured and the actual wavefronts agree, were investigated (not shown). For these instances, the instantaneous SRA appears to be valid (pressure/total fluctuations are small) and no significant vortical activity in the boundary layer was observed.

CONCLUSIONS

A complimentary experimental technique, which uses simultaneous velocity-wavefront measurements, is proposed. To demonstrate the technique, simultaneous wavefront/velocity measurements were performed in the low subsonic moderately-heated boundary layer at Caltech and in the compressible subsonic adiabatic boundary layer at University of Notre Dame. Since wavefronts are proportional to the integrated density field, it was shown that the comparison between the velocity field and the wavefront provide additional information about the large-scale structures inside the boundary layer. Plausible relations between different structures in the boundary layer and the corresponding wavefronts were presented and discussed. It was proposed that Malley probe 1-D wavefronts can be used to solve the inverse problem of relating integral optical distortions to vortical structures. 2-D wavefronts were shown to provide additional information about the streamwise/spanwise statistics of the large-scale BL structures. By comparing actual wavefronts with the estimated ones, using the Strong Reynolds Analogy, the effect of the local pressure field and the underlying structure can be estimated and studied.

ACKNOWLEDGEMENTS

The support of the Department of Defense through the National Defense Science & Engineering Graduate Fellowship (NDSEG) Program and the Air Force Office of Scientific Research Grant # FA9550-12-1-0060 are gratefully acknowledged. The U.S. Government is authorized to reproduce and distribute reprints for governmental purposes notwithstanding any copyright notation thereon.

REFERENCES

Adrian. R.J. 2007 Hairpin vortex organization in wall turbulence. *Phys. Fluids*, **19**(4), pp. 1-16.

Cress, J., *Optical Aberrations Caused by Coherent Structures in a Subsonic, Compressible, Turbulent Boundary Layer*, Ph.D. thesis, U. of Notre Dame, 2010.

Elsinga, G.E., Scarano, F., Wieneke, B. and Van Oudheusden, BW.," Tomographic particle image velocimetry", *Exp. in Fluids*, **41**(*6*), 933-947, 2006.

Fahringer, T., Thurow, B.," Tomographic Reconstruction of a 3-D Flow Field Using a Plenoptic Camera", AIAA Paper 2012-2826, 2012.

Fitzgerald, E.J. & Jumper, E.J. „The optical distortion mechanism in a nearly incompressible free shear layer," *J. Fluid Mech*. **512**, 153–89, 2004

Gordeyev, S., Smith, A.E., Cress, J.A. and Jumper E.J., "Experimental studies of aero-optical properties of subsonic turbulent boundary layers," *Journal of Fluid Mechanics*, **740**, pp 214-253, 2014.

Gordeyev, S., Cress, J.A,, Smith, A.E. and Jumper. E.J., "Aero-Optical Measurements in a Subsonic, Turbulent Boundary Layer with Non-Adiabatic Walls," to appear in *Physics of Fluids*, 2015.

Hutchins, N., Hambleton, W.T. & Marusic I. 2005 Inclined Cross-Stream Stereo Particle Image Velocimetry Measurements in Turbulent Boundary Layers. *J. Fluid Mech.*, **541**, pp.21-34.

Marusic, I., McKeon, B. J., Monkewitz, P. A., Nagib, H. M., Smits, A. J. & Sreenivasan, K. R. 'Wall-bounded turbulent flows: recent advances and key issues' *Phys. Fluids*, **22**, 65103, 2010.

Morkovin, M.V. 1962 Effects of compressibility on turbulent flows. in *Mechanique de la Turbulence* (ed. By A. Favre), CNRS, pp. 367-380, Paris, France.

Platt, B. and Shack, R., "History and principles of Shack-Hartmann wavefront sensing," *J. Refract. Surg.* **17**(*5*), 573–577, 2001.

Smits, A. J., McKeon, B. J. and Marusic, I. 'High Reynolds number wall turbulence' *Annual Review of Fluid Mechanics*, **43**, 353-375, 2011.

Smith. A.E. *Evaluation of Passive Boundary Layer Flow Control Techniques for Aero-Optic Mitigation*, PhD. Thesis, U. of Notre Dame, 2015.

Sutton, G.W., "Effect of turbulent fluctuations in an optically active fluid medium." *AIAA Journal*, **7**(*9*), 1737-1743, Sept. 1969.

Wang, M., Mani, A., and Gordeyev, S., "Physics and Computation of Aero-Optics", *Annual Review of Fluid Mechanics*, Vol. 44, pp. 299-321, 2012.

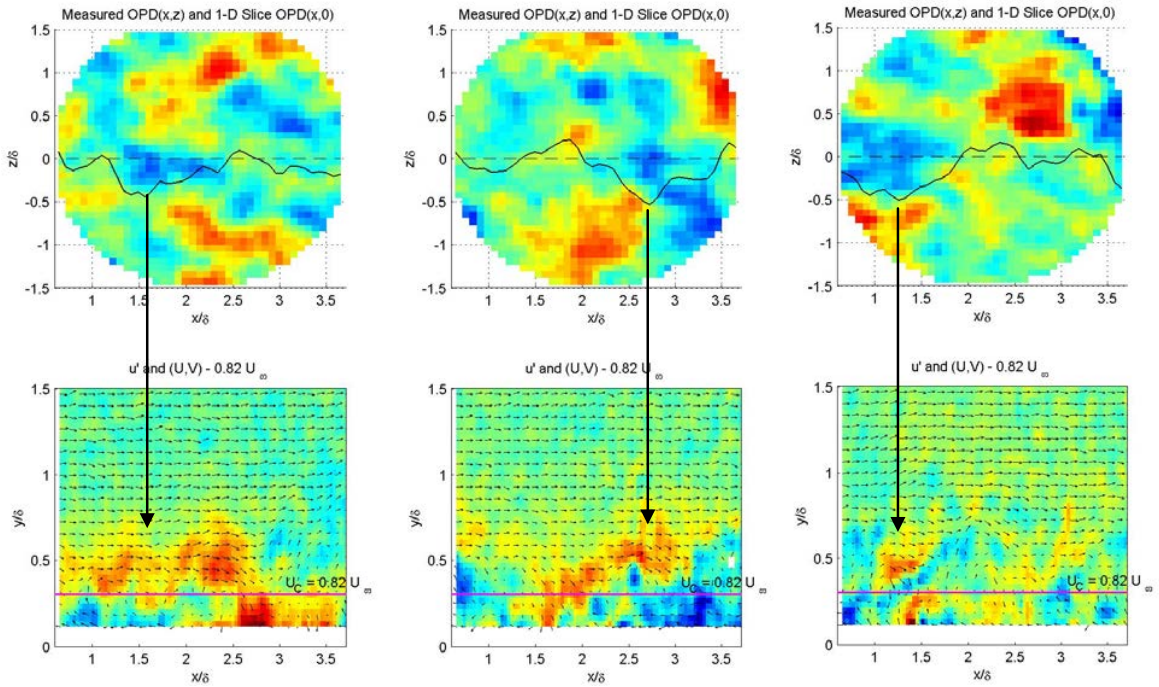

Figure 5. Top: Representative wavefronts with *local minima* near the PIV centerline (dashed line). Measured 2-D *OPD* are given by false color map, blue are negative values and red are positive values, and the measured 1-D *OPD*(*x*,0) slices are shown as black lines. Bottom: the corresponding velocity fields. Velocity vectors are the instantaneous *U*-velocity with $0.82U_\infty$ subtracted, superimposed with the instantaneous fluctuating *u*-field (false color map, blue are negative values and red are positive values). Solid magenta line indicates a *y*-location, where the local mean *U*-velocity is 0.82 of the freestream speed.

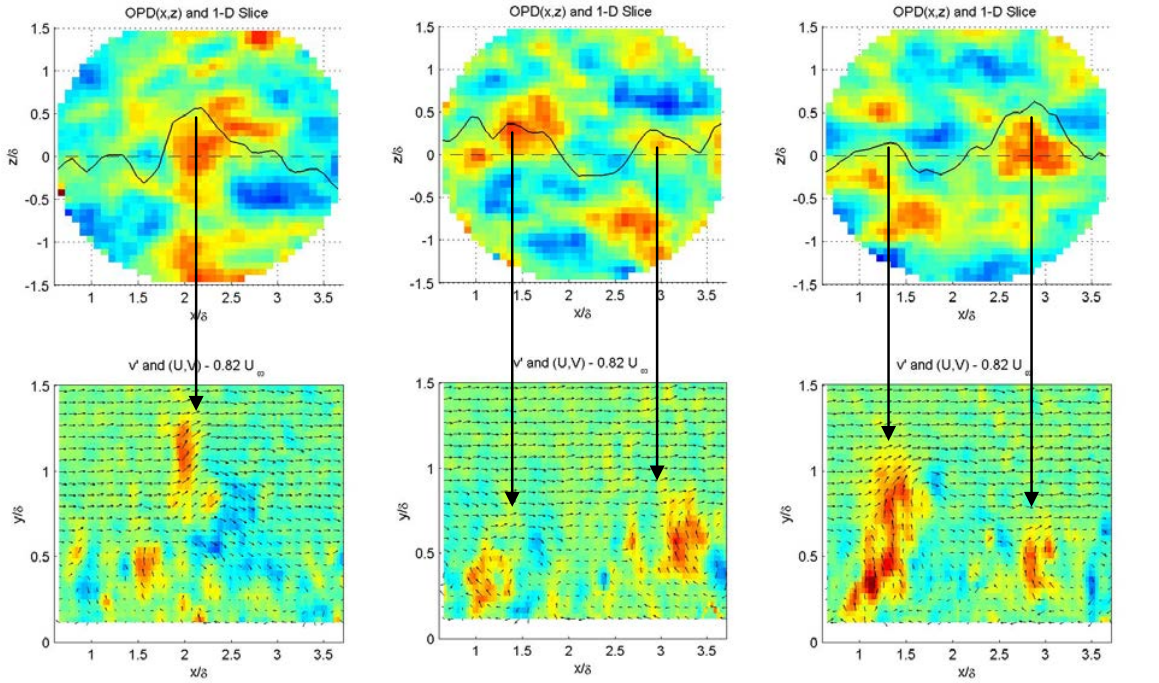

Figure 6. Top: Representative wavefronts with *local maxima* near the PIV centerline (dashed line). Measured 2-D *OPD* are given by false color map, blue are negative values and red are positive values, and the measured 1-D *OPD*(*x*,0) slices are shown as black lines. Bottom: the corresponding velocity fields. Velocity vectors are the instantaneous *U*-velocity with $0.82U_\infty$ subtracted, superimposed with the instantaneous fluctuating *v*-field (false color map, blue are negative values and red are positive values)